AFRL-SN-RS-TR-1998-82
Final Technical Report
May 1998

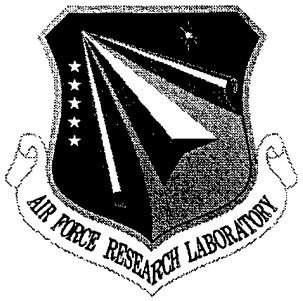

FREE-CARRIER GRATING DIFFRACTION FROM QUANTUM WELL FABRY-PEROTS

Purdue Research Foundation

David D. Nolte and M. R. Melloch

APPROVED FOR PUBLIC RELEASE; DISTRIBUTION UNLIMITED.

AIR FORCE RESEARCH LABORATORY
SENSORS DIRECTORATE
ROME RESEARCH SITE
ROME, NEW YORK

This report has been reviewed by the Air Force Research Laboratory, Information Directorate, Public Affairs Office (IFOIPA) and is releasable to the National Technical Information Service (NTIS). At NTIS it will be releasable to the general public, including foreign nations.

AFRL-SN-RS-TR-1998-82 has been reviewed and is approved for publication.

APPROVED: George Brost

GEORGE A. BROST
Project Engineer

FOR THE DIRECTOR: Robert G. Polce

ROBERT G. POLCE, Acting Chief
Rome Operations Office
Sensors Directorate

If your address has changed or if you wish to be removed from the Air Force Research Laboratory Rome Research Site mailing list, or if the addressee is no longer employed by your organization, please notify AFRL/SNDR, 25 Electronic Pky, Rome, NY 13441-4515. This will assist us in maintaining a current mailing list.

Do not return copies of this report unless contractual obligations or notices on a specific document require that it be returned.

REPORT DOCUMENTATION PAGE	Form Approved OMB No. 0704-0188

1. AGENCY USE ONLY *(Leave blank)*	2. REPORT DATE	3. REPORT TYPE AND DATES COVERED
	May 1998	FINAL Jul 96 - Jul 97

4. TITLE AND SUBTITLE
FREE-CARRIER GRATING DIFFRACTION FROM QUANTUM WELL FABRY-PEROTS

5. FUNDING NUMBERS
C - F30602-96-2-0033
PE - 62702F
PR - 4600
TA - P5
WU - PC

6. AUTHOR(S)
David D. Nolte and M. R. Melloch

7. PERFORMING ORGANIZATION NAME(S) AND ADDRESS(ES)
Purdue Research Foundation
1063 Hovde Hall
West Lafayette IN 47907

8. PERFORMING ORGANIZATION REPORT NUMBER
N/A

9. SPONSORING/MONITORING AGENCY NAME(S) AND ADDRESS(ES)
Air Force Research Laboratory/SNDR
25 Electronic Pky
Rome NY 13441-4515

10. SPONSORING/MONITORING AGENCY REPORT NUMBER
AFRL-SN-RS-TR-1998-82

11. SUPPLEMENTARY NOTES
Project Engineer: George Brost, SNDR, (315) 330-7669

12a. DISTRIBUTION AVAILABILITY STATEMENT
Approved for public release; distribution unlimited.

12b. DISTRIBUTION CODE

13. ABSTRACT *(Maximum 200 words)*
This effort investigated the possibility of replacing the electroabsorption quantum wells with the strong absorption bleaching nonlinearities of high peak-power pulses. Free carrier absorption bleaching was investigated in GaAs epilayers and AlGaAs/GaAs multiple quantum wells for excitation from above bandgap 10 ns pulses. Grating diffraction was also measured. The presence of thermal gratings, due to heating from the high-intensity pump pulse, contributed significantly to the observed diffraction. The lower than expected observed diffraction efficiency was attributed to a reduction in the internal writing efficiency due to the comparable sizes of the diffusion lengths and the grating space.

14. SUBJECT TERMS
photorefraction, Multiple Quantum Wells (MQW), diffraction

15. NUMBER OF PAGES
28

16. PRICE CODE

17. SECURITY CLASSIFICATION OF REPORT	18. SECURITY CLASSIFICATION OF THIS PAGE	19. SECURITY CLASSIFICATION OF ABSTRACT	20. LIMITATION OF ABSTRACT
UNCLASSIFIED	UNCLASSIFIED	UNCLASSIFIED	UL

TABLE OF CONTENTS

LIST OF FIGURES

1. Introduction

Semiconductor microcavities[1] display a variety of interesting behaviors and are suited to many applications. For example, the modification of electromagnetic modes in microcavity resonators is the basis for the design of semiconductor lasers and devices which rely on strong cavity quantum electrodynamic effects. Incorporation of an absorbing material within a cavity bounded by mirrors leads to modifications in both the amplitude and phase of the optical wave modes. A small number of modes of the optical field can be isolated with careful control of the cavity geometry and size[2]. By tailoring the thickness and end reflectivities of the cavity, the spontaneous emission into certain modes may be enhanced or suppressed[3-6] to improve lasing efficiency. Multiple passes of the high-Q cavity are required in order to build up gain within the lasing medium, which typically consists of only a few quantum wells and is on the order of $\lambda/2n$ in thickness (~100nm). A key feature of much of this work is operation at low temperatures requiring liquid nitrogen or liquid helium. Microcavity resonance effects in larger, lower Q, devices, also called asymmetric Fabry-Perots[7], have been used to increase contrast ratios in electro-optic modulators[8-11], self electro-optic devices[12] (SEEDs) and for enhancement of the diffraction efficiency in photorefractive multiple quantum well devices[13, 14] that operate at room temperature.

The goal of our research is to take advantage of photorefractive quantum well asymmetric Fabry-Perots[13, 14] and replace the electroabsorption in the photorefractive quantum wells with the strong absorption bleaching nonlinearities[15] of high peak-power pulses. The resulting devices can have diffraction efficiencies that exceed the efficiencies of photorefractive quantum wells. Band-filling and exciton bleaching effects can potentially produce larger absorption changes than electro-optic effects. More importantly, absorption bleaching reduces optical absorption, providing higher transparency for the device and larger input diffraction efficiencies than electroabsorption effects. A spatial modulation of the transmittance or reflectance is caused when two coherent beams write free-carrier gratings in the quantum wells. The coherent excitation may be either in the form of continuous, highly focused laser beams, or in the form of high-peak-intensity pulses. The Fabry-Perot cavity resonance conditions can be highly sensitive to even small changes in absorption or refractive index. The structures operate without electric fields, and rely only on band-filling and exciton screening nonlinearities to produce large absorption changes. Under extreme conditions, optical gain is even possible when a sufficient population inversion has been established[15]. In this instance, it may even be possible to have net gain for a CW probe beam diffracting from the free-carrier gratings.

2. Theory of Combined Band-Edge Nonlinearity and ASFP Cavities

The key features of free-carriers are absorption bleaching and band filling[15]. Bleaching occurs when the excitonic absorption is quenched by the mechanism of phase space filling, a result of the fermionic nature of electrons and holes, and Coulomb screening. Phase space filling describes the situation when a conduction band state is occupied by an electron, blocking other electrons from that state. The exciton oscillator strength, f_n, is calculated using the transition probability from the ground state |0> to the excited states |n> by [16]

$$f_n = A\left| x_{cv} \right|^2 \left| \int_k \frac{dk}{(2\pi)^2} \chi_k^n (1 - f_k)^{1/2} \right|^2 \tag{1}$$

where A is a constant, f_k is the Fermi function,

$$f_k = \frac{1}{e^{(\varepsilon - \mu)/k_B T} + 1}, \tag{2}$$

χ_k^n is the exciton wave function, and x_{cv} is the dipolar matrix element between the conduction and valence band. Through the carrier dependence of the chemical potential, μ, the oscillator strength calculated in (1) decreases as a critical number of carriers is created, causing a resultant decrease in the excitonic absorption. Screening of the electron-hole Coulomb attraction due to the presence of large numbers of carriers also reduces the binding energy and lifetime, and therefore the absorption. At the Mott density, ~2 x 10^{18}/cm^3, above which only ionized states exist, phase space filling and Coulomb screening effects cause the exciton binding energy to vanish. Under conditions of sufficiently high carrier density the absorption can be reduced below zero, i.e. optical gain is present.

The most important difference between free-carrier effects and electroabsorption is that in the free-carrier case the absorption at the band-edge is reduced, while in the electroabsorption case the absorption extends into the bandgap. This difference is essential and could allow free-carrier gratings to produce significantly larger transient diffraction efficiencies because in the free-carrier case the refractive index changes just below the bandgap are large, but without adverse absorption. When these features are incorporated into an asymmetric Fabry-Perot where multiple beam interference effects are strong, the largest quantum well transient input diffraction efficiencies should result. The ASFP consists of an absorbing cavity with unequal front , R_T, and back, R_B, reflectivities. If the cavity is balanced according to

$$R_B e^{(-2\alpha L_c)} = R_T \tag{3}$$

total destructive interference can occur between the light reflected from the front and back reflectors.

The diffraction grating is written when two coherent light beams of intensity I_1 and I_2 at or above the band gap interfere within the material, setting up a spatially modulated light intensity

$$I = I_o(1 + m \cos Kx) \tag{4}$$

where $I_o = I_1 + I_2$, K is the grating vector length, and m is

$$m = \frac{2\sqrt{I_1 I_2}}{I_1 + I_2} \tag{5}$$

If the grating beams are of sufficient intensity, large numbers of carriers are generated. In order to see significant absorption and refractive index changes due to the presence of the free carriers, a density on the order of $10^{18}/cm^3$ is required. The spatially modulated absorption and index creates the diffraction grating which can then self-diffract one of the grating beams if it is near the band edge. Alternatively, a separate probe beam tuned to the band edge can be diffracted if the grating is written by above bandgap beams. The first order diffraction efficiency of a cavity of thickness L is given by

$$\eta_1 \propto e^{(-\bar{\alpha}L/\cos(\theta'))}\left[\left(\frac{2\pi n_1 L}{\lambda\cos(\theta')}\right)^2 + \left(\frac{\alpha_1 L}{2\cos(\theta')}\right)^2\right] \tag{6}$$

where $\bar{\alpha}$ is the average absorption coefficient during mixing, λ is the probe beam wavelength, θ' is the incident angle, and n_1 and α_1 are the first Fourier coefficients of the modulated refractive index and absorption, respectively, given by

$$\alpha = \alpha_o + \alpha_1 \cos(Kx) \tag{7}$$

and

$$n = n_o + n_1 \cos(Kx). \tag{8}$$

The Fourier coeefficiencts of the absorption and index gratings are proportional to a modified modulation index, $\tilde{m} = m\,\xi$ taking into account the internal grating writing efficiency, ξ, in the material which is a function of the diffusion, carrier density, temperature, and grating spacing. This writing efficiency

$$\xi \propto \frac{1}{1 + K^2 L_D^2} \tag{9}$$

where K is the grating vector length, and L_D is the diffusion length, decreases the diffraction efficiency by a factor of ξ^2 through the index and absorption dependence.

We have simulated the ASFP response for a free carrier grating with $\xi=1$ compared with the best predicted performance of the longitudinal geometry photorefractive quantum well in Fig. 1. A peak transient input diffraction efficiency of 13% is predicted compared to 6% for the photorefractive quantum well. Because of the sharp low-energy absorption edge in the free-carrier case, the diffraction efficiency remains large even for large detuning of the Fabry-Perot fringes from the band-edge. The smallest diffraction efficiency for the free-carrier case is 2% under identical conditions to Fig. 1, but with a least-optimum device thickness. The maximum and minimum responses are shown in Fig. 2.

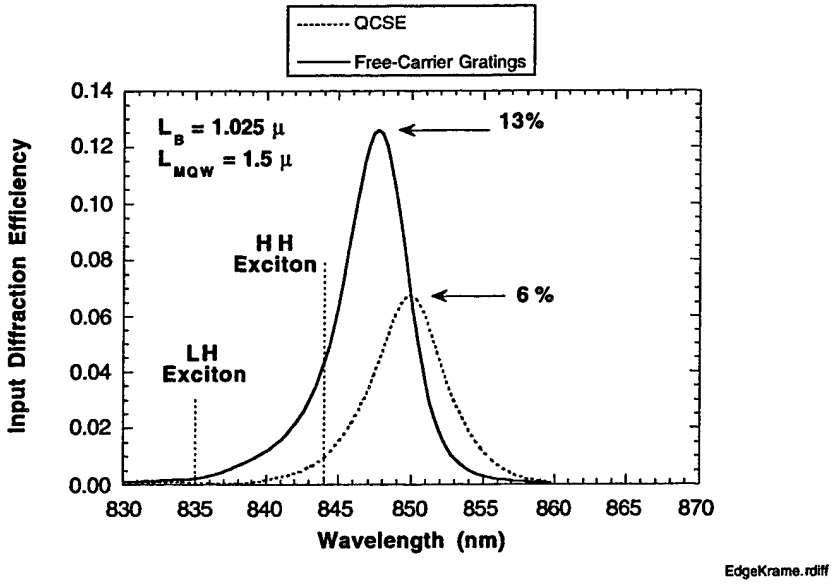

Fig. 1. Comparison of diffraction from identical ASFP for free-carrier gratings and electroabsorption gratings (longitudinal-field photorefractive quantum well geometry).

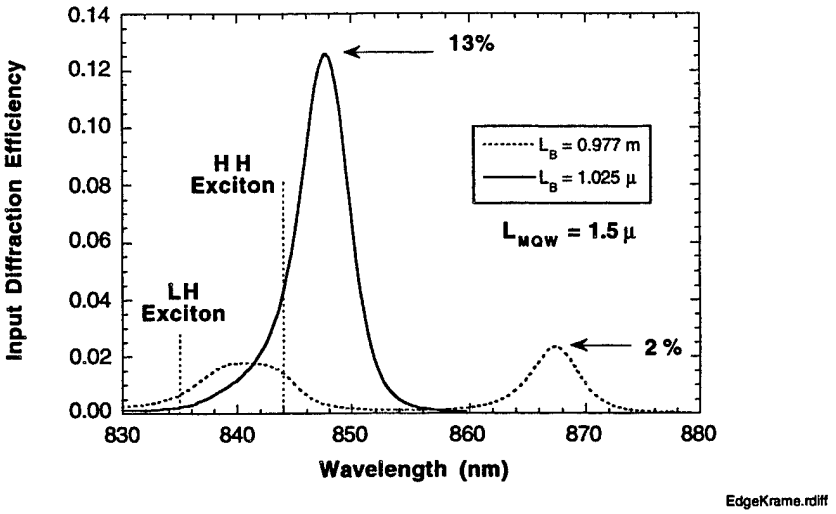

Fig. 2. Comparison of best-case and worst-case free-carrier grating in an ASFP for two different device thicknesses. The smallest diffraction efficiency from the free carrier grating is 2%.

2.1 Grating Decay Mechanisms

Several diffusion mechanisms can cause grating decay over various time frames, shown in Table 1. The grating decay lifetime τ [17], and the carrier diffusion constants D_n and D_h are given by

$$\tau = \frac{\Lambda^2}{4\pi^2 D} \qquad \text{and} \qquad D_{n,h} = \frac{\mu_{n,h} k_B T}{e} \tag{10}$$

while the diffusion length, L_D, is related to the diffusion constant by $L_D^2 = D\tau$. Surface recombination, carrier lifetime, and ballistic phonons can also decrease diffractive performance in certain cases. Diffusion processes also contribute to lowering the grating writing efficiency in (9) and can have a significant effect on the diffraction efficiency through the ξ dependence of n_1 and α_1 in (6).

Diffusion Mechanism	Diffusion Constant	Grating Lifetime[17]	Drift Length (in 1.5 μs)
Thermal	$D_{th} = 0.26\ cm^2/s$	$\tau_{th} = 0.6\ \mu s$	$L_{th} = 6.2\ \mu m$
electron (μ_n= 8000 cm^2/Vs)	$D_n = 207\ cm^2/s$	$\tau_n = 0.76\ ns$	$L_n = 176\ \mu m$
hole ($\mu_h = 400\ cm^2/Vs$)	$D_h = 10.4\ cm^2/s$	$\tau_h = 15\ ns$	$L_h = 39\ \mu m$

Table 1 Parameters for GaAs at room temperature

3. Experimental Results

3.1 Doubled Nd:YAG pump experiments

3.1.1 GaAs epilayer

In a first step towards the formation and study of gain gratings, a 1 micron thick GaAs epilayer sandwiched between two $Al_{0.3}Ga_{0.7}As$ spacer layers was bonded to a sapphire substrate. Sapphire was used in place of a glass slide to provide a superior heat sink, required due to the high pump intensities used. A pump-probe experiment was performed using a single beam from a Q-switched doubled Nd:YAG laser at 532 nm as a pump to create a large carrier density within the epilayer. A beam from a CW Ti:Sapphire laser was used to probe the epilayer at 870 nm, at the excitonic position for GaAs. The experimental setup is shown in Fig. 3 and the results in Fig. 4. A 200% change in the transmission of the probe beam due to the excitation of the free carriers is seen at a time averaged pump power of 18 mW.

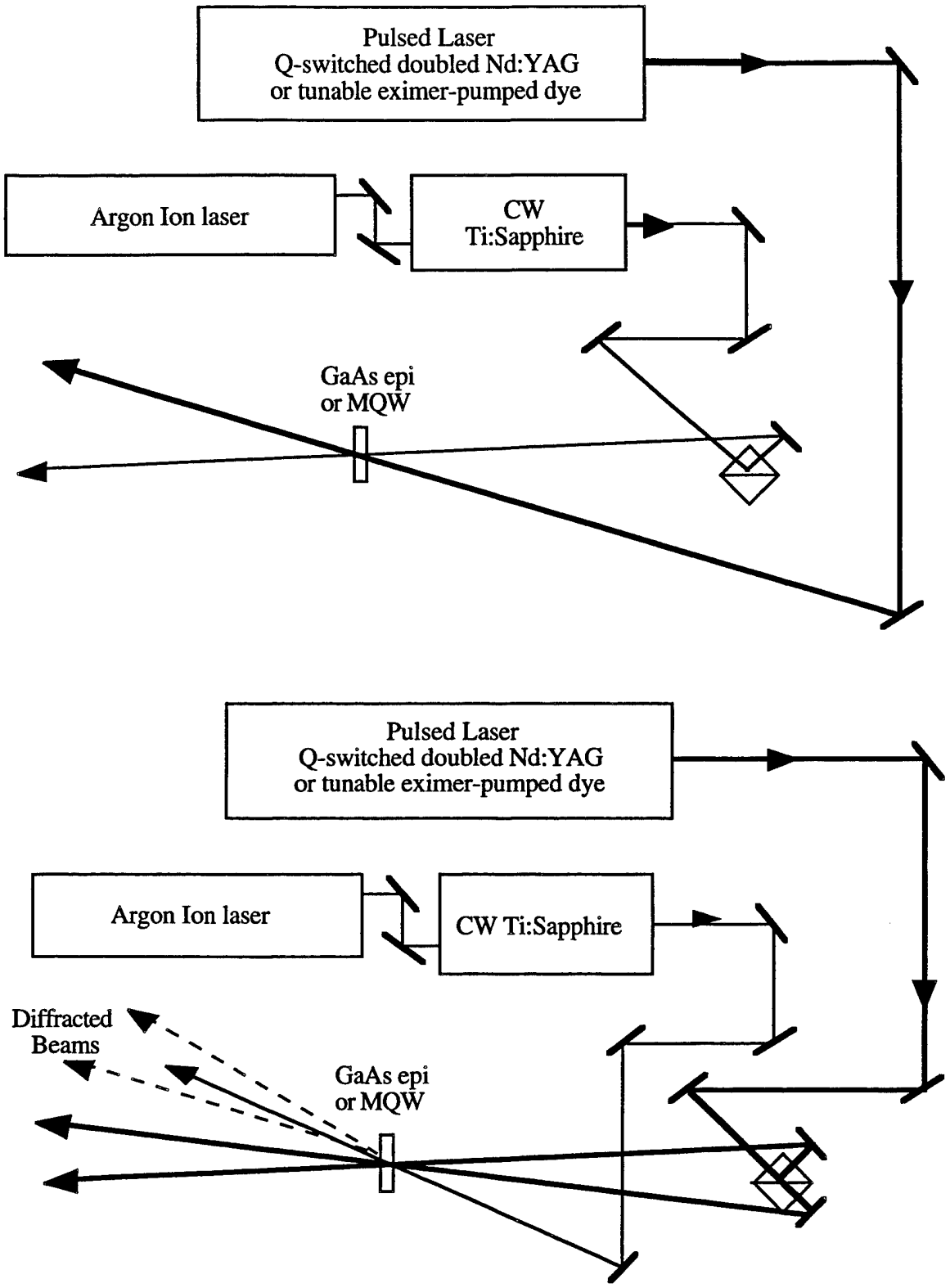

Fig. 3. Pump-probe (upper) and non-degenerate four wave mixing (lower) experimental setups.

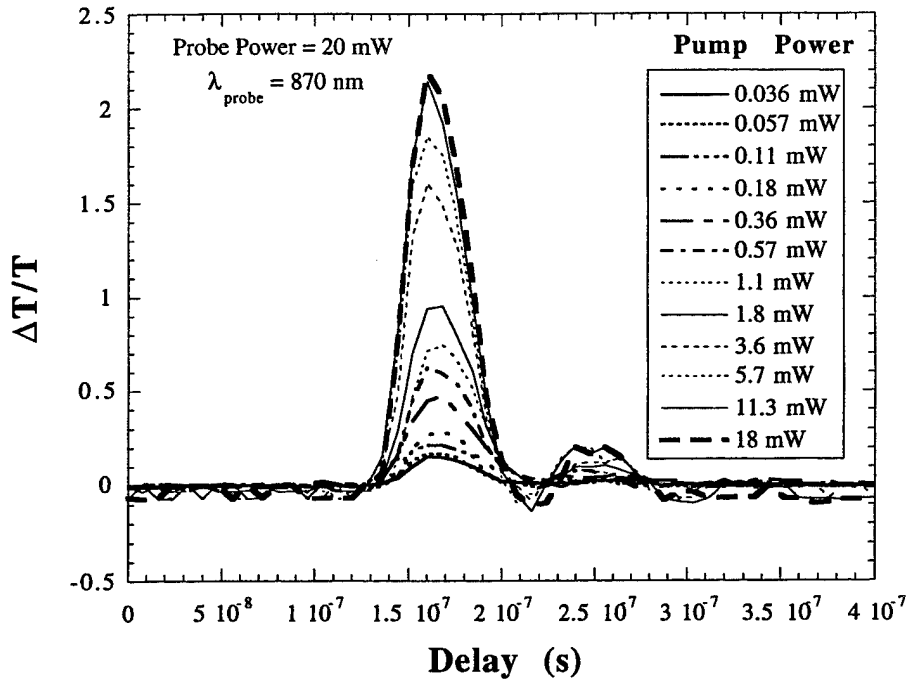

Fig. 4. Change in probe beam transmission vs. delay after Q-switch trigger pulse in a GaAs epilayer for various pump powers.

3.1.2 STG GaAs/$Al_{0.1}Ga_{0.9}As$ MQW

Pump-probe measurements of transmission change as a function of injected carriers and non-degenerate four-wave mixing have also been performed on samples of unimplanted GaAs/AlGaAs multiple quantum well (MQW) material. The device structure consisted of 114 periods of standard-temperature-grown 100 Å GaAs/75 Å $Al_{0.1}Ga_{0.9}As$ quantum wells sandwiched between $Al_{0.23}Ga_{0.77}As$ spacer layers. At the back side of the device was a 0.75 μm low temperature grown $Al_{0.23}Ga_{0.77}As$ spacer. The transmittance of this device is shown in Fig. 5.

Pump-probe measurements were performed with a 10 ns pulse Q-switched doubled Nd:YAG pump beam at 532 nm and a CW Ti:sapphire probe beam. The transmission change due to the photo-induced carriers as a function of time is shown in Fig. 6. Below the band edge at 855 nm both induced transparency and induced absorption are present, though with differing time scales. A maximum differential transmission of nearly 300% is achieved. In Fig. 7 the time scale has been increased to 50 μsec in order to fully capture the long-lived induced absorption.

In the non-degenerate four-wave mixing experiments the grating was written by 10 ns pulses from a Q-switched doubled Nd:YAG at 532 nm and was probed with a CW Ti:sapphire tuned through the band edge. A fringe spacing of 100 μm was used in an attempt to resolve the free carrier/gain grating diffraction above any grating erasure effects due to thermal diffusion. The diffractive performance is shown in Fig. 8. A slight enhancement of the diffraction is seen at 878 nm, possibly corresponding to the cavity transmittance resonance at that wavelength.

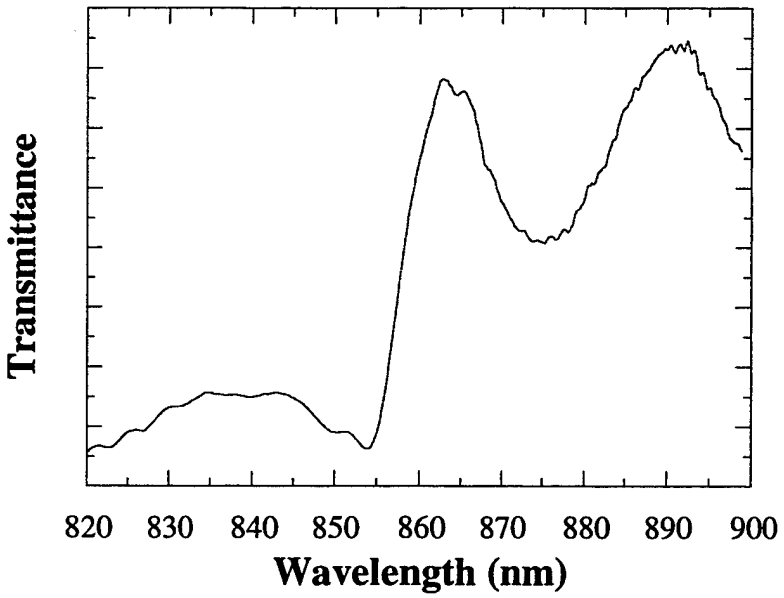

Fig. 5. Transmittance vs. wavelength of a GaAs/$Al_{0.1}Ga_{0.9}As$ MQW structure with $Al_{0.23}Ga_{0.77}As$ spacers.

The peak diffracted signal lags the 532 nm pulse by ~50 ns. Since the decay of the diffracted signal shows a linear dependence when plotted on a semi-log plot, we believe the signal, with its slow decay, to be due to the presence of a thermal grating. Grating washout due to ballistic transport of phonons generated by the 532 nm pump beams might also be decreasing the detected diffraction. Faster effects due to the presence of a carrier grating, on the order of 10 ns, are not observed, either due to washout from the strong "slow" component or to the limitations of the 10 ns rise-time photodiode used.

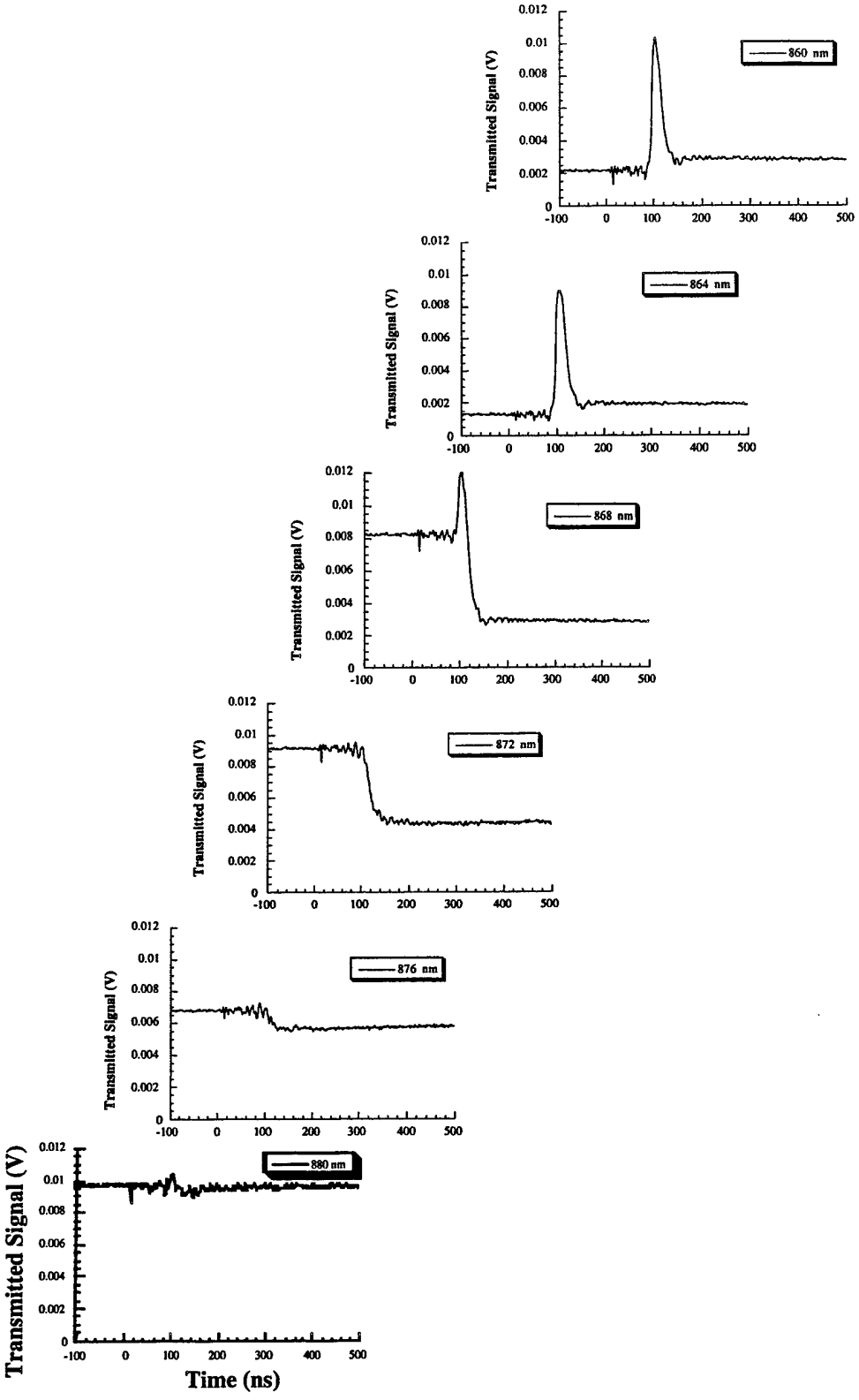

Fig. 6. Pump-probe transmission vs. time vs. CW probe wavelength on an unimplanted STG $GaAs/Al_{0.1}Ga_{0.9}As$ MQW.

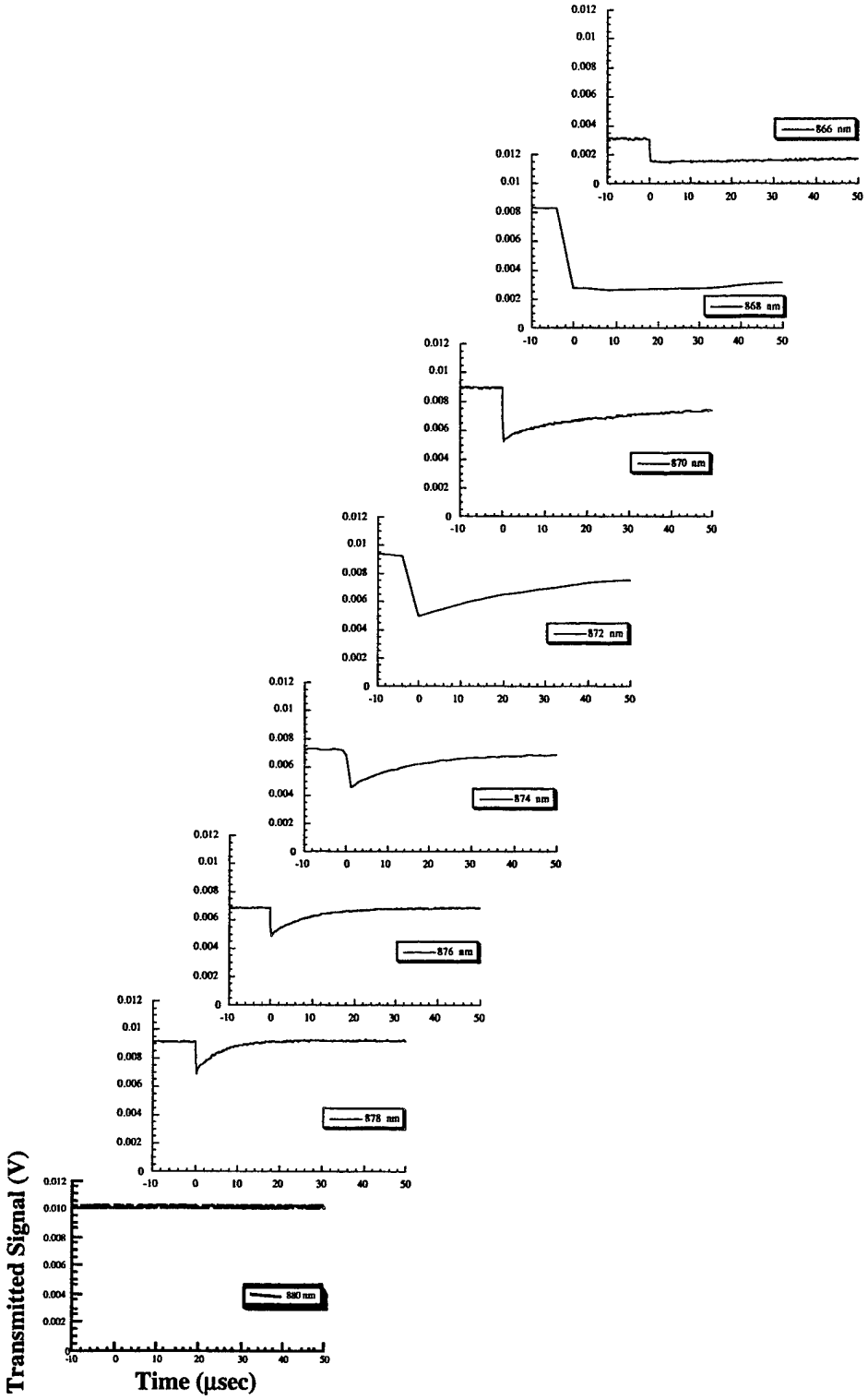

Fig. 7. Pump-Probe transmission vs. time on an expanded time scale relative to the data in Fig. 6.

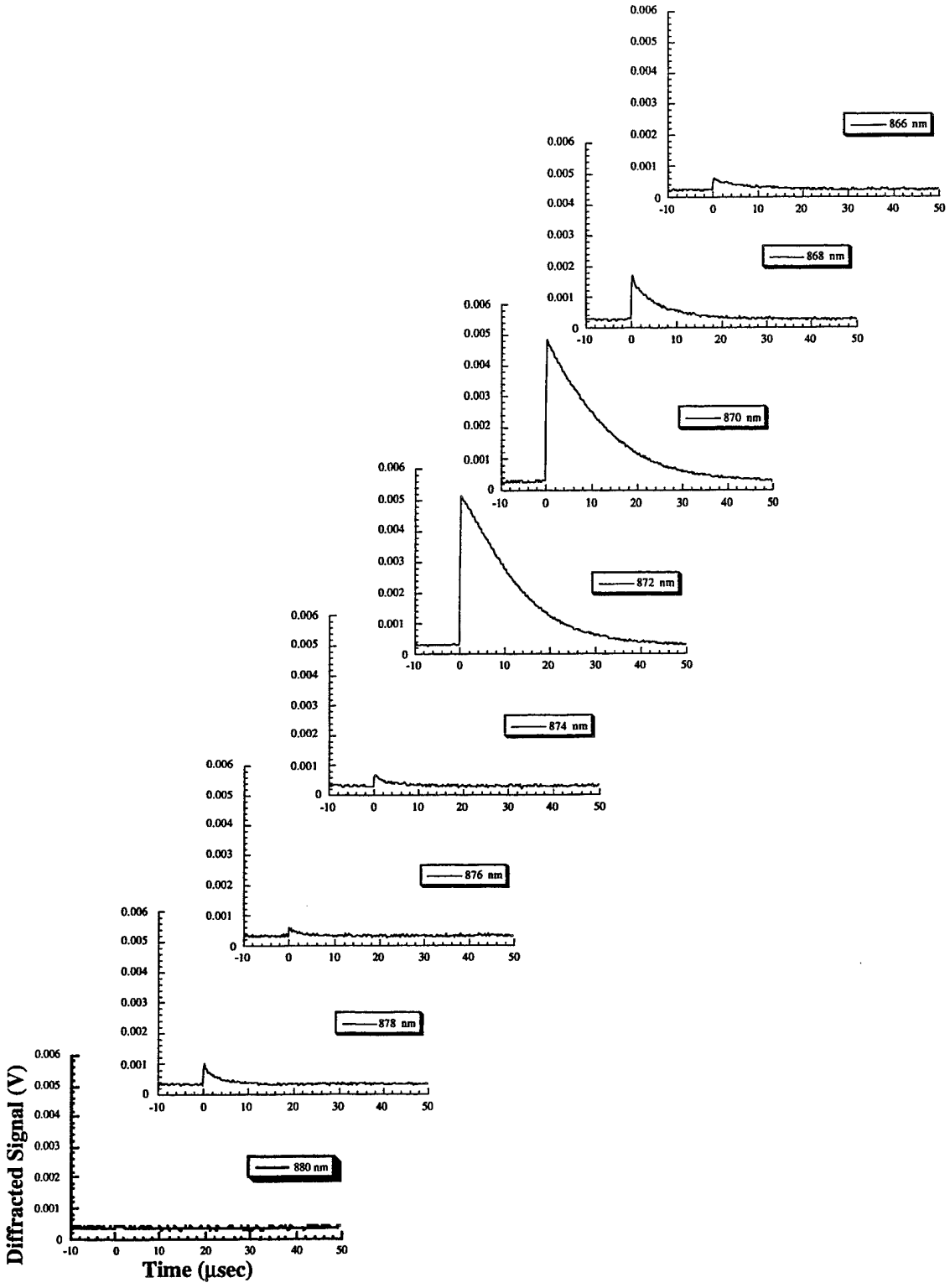

Fig. 8. Diffracted signal vs. time. vs. CW probe wavelength for STG GaAs/$Al_{0.1}Ga_{0.9}As$ MQW for a pump energy of ~ 1.75 mJ/pulse and a fringe spacing of 100 μm.

3.1.3 Gain Gratings

Since the previous experiments did not lend themselves to clear identification of gain, an additional experiment was performed on the STG GaAs/$Al_{0.1}Ga_{0.9}As$ MQW device utilizing the 10 ns 532 nm Q-switched pulse as a pump on a sample illuminated by a grating from the Ti:Sapphire tuned near the heavy-hole exciton resonance at 854 nm. In this experiment, diffraction of the Ti:sapphire beam would be the result of gain induced by the 532 nm pump. The grating spacing was 20 μm and pump beam energies of 0.01 mJ/pulse, 0.1 mJ/pulse, and 1 mJ/pulse were used. The incident direction of the 532 nm beam was varied from collinear with one Ti:sapphire grating beam to incidence at the first order diffraction angle, to possibly pick up gain or amplified spontaneous emission directed along the diffraction direction by microcavity resonance effects[2]. No diffracted signal was seen although the high speed detection requirements limited the resolution of the input diffraction efficiency to a minimum of 10^{-5}. It is probable that, in order for diffraction to be seen, the carrier density created by the Ti grating beams would need to be about the same order of magnitude as that produced by the 532 nm pump. This might be achieved by use of a mode-locked Ti:sapphire to write the gratings[18-21].

3.1.4 Reflection Geometry STG GaAs/$Al_{0.1}Ga_{0.9}As$

Diffraction due to free carrier effects has also been investigated in an unimplanted STG GaAs/$Al_{0.1}Ga_{0.9}As$ MQW structure identical to the one described previously with the addition of a dielectric mirror stack on the back side to enhance cavity resonance effects. The experimental reflectances of this structure for two separate $Al_{0.23}Ga_{0.77}As$ spacer thicknesses are shown in Fig. 9. The cavity resonance conditions for the two devices are nearly a half fringe spacing apart. Non-degenerate four-wave mixing experiments with Q-switched 2 mJ 10 ns 532 nm pump beams were performed and the results shown in Fig. 10. The cavity resonance effects on the spectral lineshape of the diffraction efficiency are clearly evident. Significant broadening of the diffractive lineshape can be achieved with the use of the correct cavity resonance position. The peak diffraction efficiency is relatively unaffected and the expected diffraction enhancement calculated in section 2 is not seen.

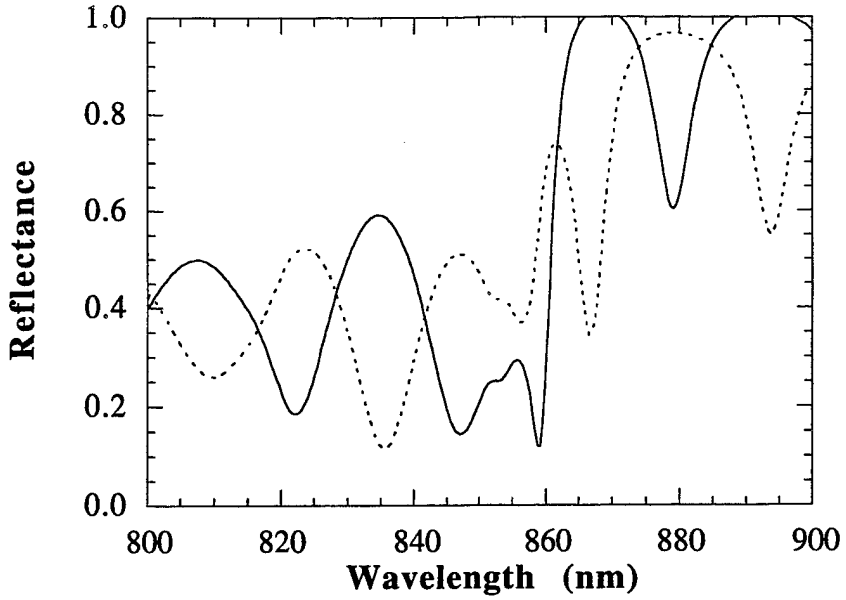

Fig. 9. Reflectance vs. wavelength of $Al_{0.1}Ga_{0.9}As/GaAs$ MQW structure w/ dielectric reflector coating. The dashed and solid lines correspond to samples with different $Al_{0.23}Ga_{0.77}As$ spacer thicknesses.

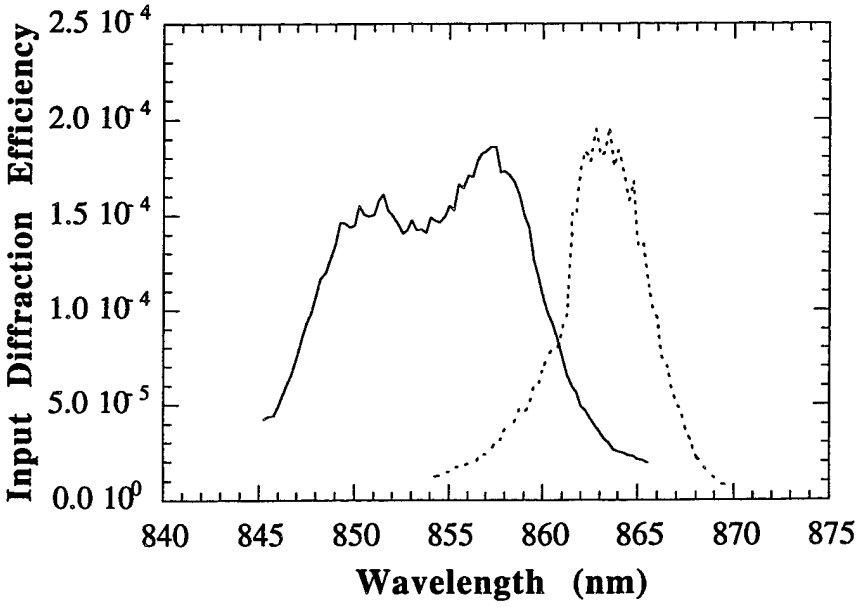

Fig. 10. Input diffractive performance of $Al_{0.1}Ga_{0.9}As/GaAs$ MQW devices in Fig. 9. Solid and dashed lines correspond to the respective reflectances in Fig. 9.

3.2 Tunable Pulsed-Dye Pump Experiments

Pumping at or near the band edge to reduce ballistic phonon effects was achieved with a ~15 ns pulse XeCl excimer-pumped tunable dye laser using Pyridine 2 dye lasing at 730 nm. A GaAs double heterostructure device consisting of 1 μm of GaAs sandwiched between two $Al_{0.3}Ga_{0.7}As$ spacers was bonded to glass to study the free carrier effects. The $Al_{0.3}Ga_{0.7}As$ spacers, with a band energy of 1.8 eV, 100 meV above the pump beam energy, were designed to eliminate surface recombination effects. The experimental setups for pump-probe and mixing are the same as in Fig. 3 with the addition of a lens to partially focus the Ti:sapphire probe onto the sample. Results of pump-probe experiments on the GaAs epilayer structure are shown in Fig. 11. Clear bleaching of the excitonic absorption is seen above the bandedge, which has been shifted to lower energy due to heating from the pump beam.

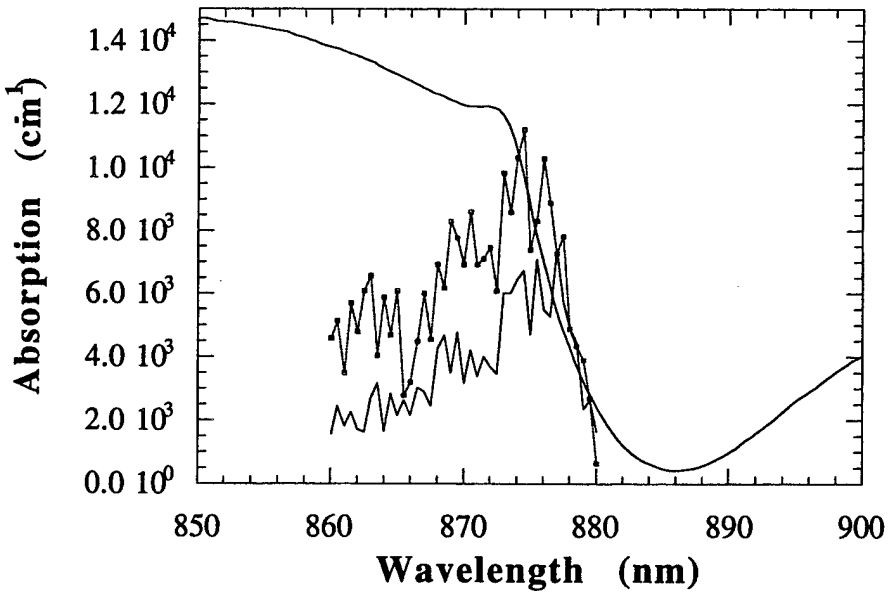

Fig. 11. GaAs absorption (solid line) and bleaching for 730 nm pump beam energies of 0.35 mJ/pulse (circles), and 3.5 mJ/pulse (crosses) pump energy.

The diffraction from the GaAs epilayer is shown in Fig. 12. A peak value of nearly $4x10^{-3}$ is achieved. The signal is composed of a "fast" peak with a FWHM of ~50-100 ns and a "slow" exponentially decaying component with a lifetime of ~1.5 μs. A comparison with Table 1 shows the "fast" component to have a comparable lifetime to carrier diffusion, taking into account the

resolution limitations of our 8 ns rise-time photodetector, and 400 MHz bandwidth oscilloscope, while the "slow" component can be associated with washout of a thermal grating. A dramatic enhancement of the "slow" component occurs near a probe wavelength of 900 nm. A portion (~15 nm) of the 30 nm shift of this enhancement above the GaAs bandedge is due to heating effects from the intense Ti:sapphire probe beam. Further shifting of the bandedge occurs due to heating from the pump pulse. A ~150° rise from the 3.5 mJ pump pulse is calculated, from parameters in Table 2, to shift the band edge an additional 15 nm to ~905 nm.

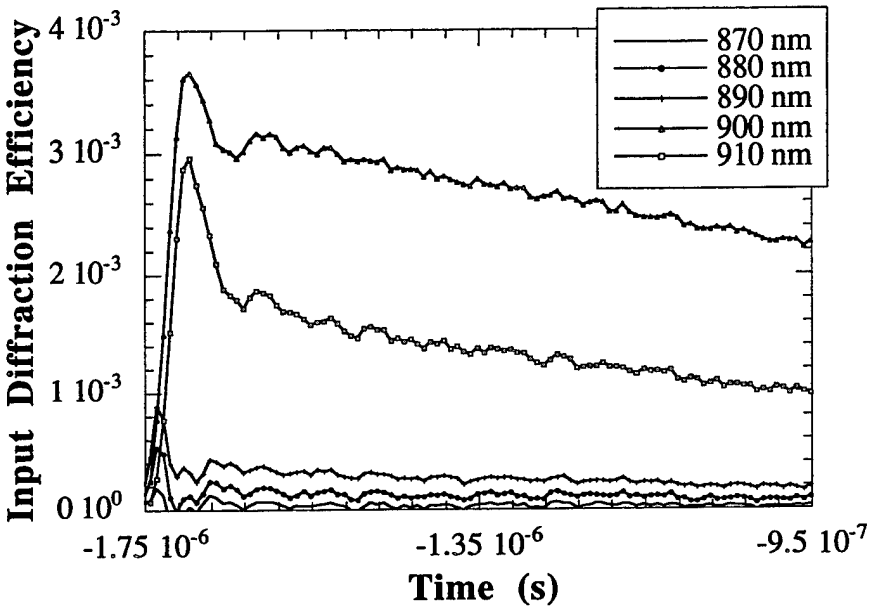

Fig. 12. Input diffractive performance of GaAs epilayer. The 730 nm grating pump energy was ~3.5 mJ/pulse with a fringe spacing of 25 μm.

sample mass	Specific Heat C_p	$dE_g\Gamma/DT$	E_{pulse}
1.34×10^{-4} g	0.335 J/g deg[22]	-3.95×10^{-4} eV/deg[22]	3.5 mJ

Table 2 GaAs parameters for bandedge shift calculation

The linear decay of the diffractive signal was dependent on the overlap between the grating beams and the Ti:sapphire probe beam as shown in Fig. 13. This is attributed to the change in grating shape, and the resulting change in the thermal profile created within the device due to the varied interference between the beams.

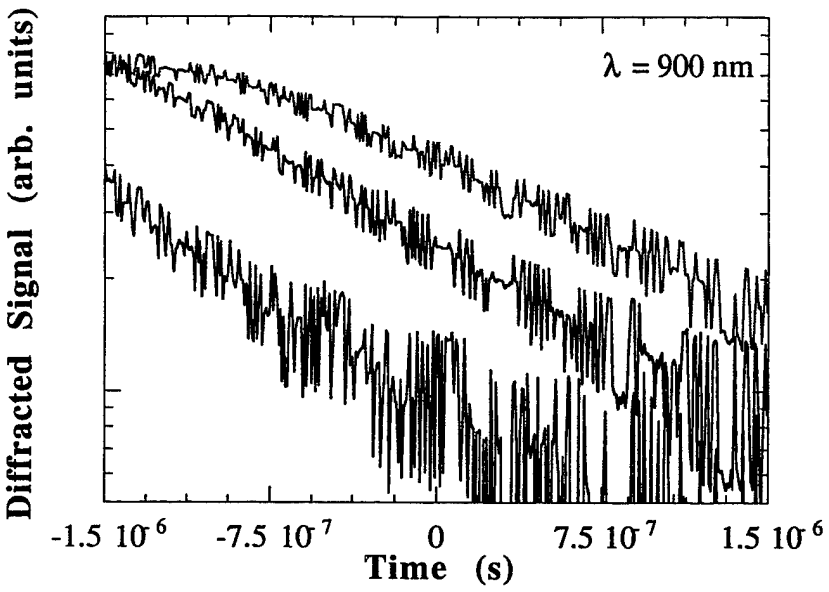

Fig. 13. Diffracted signal from a GaAs epilayer vs. 730 nm pump beam overlap.

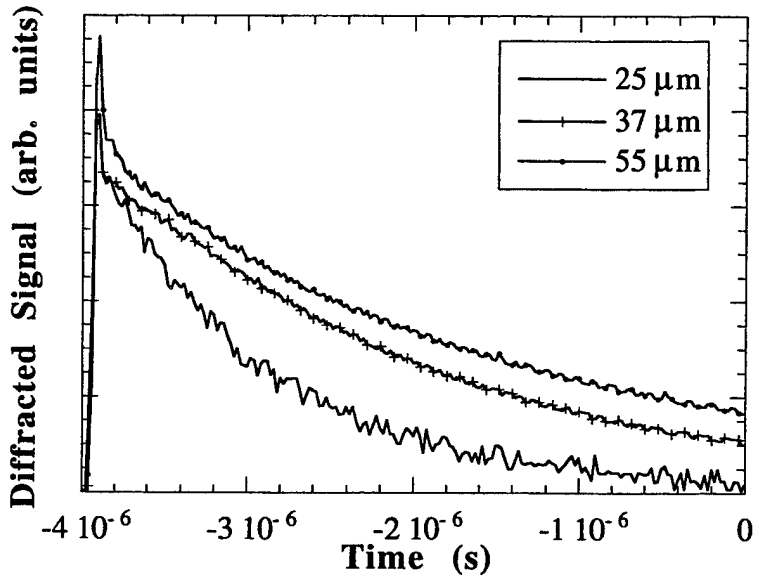

Fig. 14. Diffracted signal at a probe wavelength of 900 nm and grating pump beam energy of ~3.5 mJ/pulse from a GaAs epilayer vs. grating fringe spacing

The diffracted signal decay time vs. fringe spacing is shown in Fig. 14. As the fringe spacing is doubled the signal lifetime changes from 1.5 μs to 3.0 μs. If the process of thermal diffusion was responsible for this slow decay, a square dependence on Λ would be expected. The deviation from this dependence may be partially due to the large error bars of this measurement.

4. Discussion and Future

Free carrier absorption bleaching has been investigated in GaAs epilayers and AlGaAs/GaAs MQWs due excitation by above bandgap 10 ns pulses. Significant bleaching of the absorption is observed with associated thermal effects due to heating from the high-intensity pump pulses. Diffraction from gratings created from these pulses shows these thermal effects are significant. In fact, the portion of the diffraction attributed to the presence of a thermal grating contributes most of the observed diffraction efficiency. A lower than expected overall diffraction efficiency for both the GaAs epilayers and the GaAs/AlGaAs MQWs is attributed to a reduction in internal writing efficiency, ξ, due to the comparable sizes of the diffusion lengths and the grating spacings. A ξ of only 0.22 would account for the observed 1.5 order of magnitude lower diffraction efficiency as compared with the calculations in Section 2. Free carrier diffraction dynamics in these semiconductor microcavity structures can be further resolved with the use of a faster rise-time detector and longer fringe spacings. Additional devices such as a high-Q cavity consisting of a MQW or GaAs epilayer sandwiched between 2 Bragg stacks promise to yield higher diffraction efficiencies and possibly even room temperature gain by allowing multiple passes through the active region.

5. References

[1] Y. Yamamoto and R. E. Slusher, "Optical Processes in Microcavities," in *Physics Today*, 1993, pp. 66.

[2] G. Bjork, K. Igeta, S. Machida, and Y. Yamamoto, "Modification of the spontaneous emission rate in planar dielectric microcavity structures," *Phys. Rev. A*, vol. 43, pp. 669, 1991.

[3] E. M. Purcell, "Spontaneous emission probabilities at radio frequencies," *Phys. Rev.*, vol. 69, pp. 681, 1946.

[4] D. Kleppner, "Inhibited spontaneous emission," *Phys. Rev. Lett.*, vol. 47, pp. 233, 1981.

[5] E. Yablonovitch, "Inhibited spontaneous emission in solid-state physics and electronics," *Phys. Rev. Lett.*, vol. 58, pp. 2059, 1987.

[6] Y. Yamamoto and S. Machida, "Microcavity semiconductor laser with enhanced spontaneous emission," *Phys. Rev. A*, vol. 44, pp. 657, 1991.

[7] R. H. Yan, R. J. Simes, and L. A. Coldren, "Electroabsorptive Fabry-Perot reflection modulators with asymmetric mirrors," *IEEE Phot. Tech. Lett.*, vol. 1, pp. 273, 1989.

[8] R.-H. Yan, R. J. Simes, and L. A. Coldren, "Analysis and design of surface-normal Fabry-Perot electrooptic modulators," *IEEE J. Quant. Electron.*, vol. 25, pp. 2272, 1989.

[9] G. Livescu, G. D. Boyd, R. A. Morgan, L. M. F. Chirovsky, A. M. Fox, R. E. Leibenguth, M. T. Asom, and M. W. Focht, "Role of electrorefraction in quantum-well Fabry-Perot modulators," *Appl. Phys. Lett.*, vol. 60, pp. 1418, 1992.

[10] B. Pezeshki, G. A. Williams, and J. S. Harris Jr., "Optical phase modulator utilizing electroabsorption in a Fabry-Perot cavity," *Appl. Phys. Lett.*, vol. 60, pp. 1061, 1992.

[11] J. F. Heffernan, M. H. Moloney, J. Hegarty, J. S. Roberts, and M. Whitehead, "All optical high contrast absorptive modulation in an asymmetric Fabry-Perot etalon," *Appl. Phys. Lett.*, vol. 58, pp. 2877, 1991.

[12] K.-K. Law, R. H. Yan, L. A. Coldren, and J. L. Merz, "Self-electro-optic device based on a superlattice asymmetric Fabry-Perot modulator with an on/off ratio > 100:1," *Appl. Phys. Lett.*, vol. 57, pp. 1345, 1990.

[13] K. M. Kwolek, M. R. Melloch, and D. D. Nolte, "Dynamic holography in a reflection/transmission photorefractive quantum-well asymmetric Fabry-Perot," *Appl. Phys. Lett.*, vol. 65, pp. 385, 1994.

[14] K. M. Kwolek, M. R. Melloch, and D. D. Nolte, "Photorefractive Asymmetric Fabry-Perot quantum wells: Transverse-Field Geometry," *Appl. Phys. Lett.*, vol. 67, pp. 736, 1995.

[15] H. Haug and S. W. Koch, *Quantum Theory of the Optical and Electronic Properties of Semiconductors*. Singapore: World Scientific, 1990.

[16] R. J. Elliot, "Intensity of optical absorption by excitons," *Phys. Rev.*, vol. 108, pp. 1384, 1957.

[17] R. K. Jain and M. B. Klein, "Degenerate four-wave mixing near the band gap of semiconductors," *Appl. Phys. Lett.*, vol. 35, pp. 454, 1979.

[18] W. H. Knox, R. L. Fork, M. C. Downer, D. A. B. Miller, D. S. Chemla, C. V. Shank, A. C. Gossard, and W. Wiegmann, "Femtosecond dynamics of resonantly excited excitons in room-temperature GaAs quantum wells.," *Phys. Rev. Lett.*, vol. 54, pp. 1306, 1985.

[19] P. M. Fauchet and T. Gong, "Femtosecond dynamics of hot-carriers in GaAs," *Proc. of SPIE*, vol. 1677, pp. 25, 1992.

[20] D. Birkedal, V. G. Lyssenko, J. M. Hvam, and K. E. Sayed, "Continuum contribution to excitonic four-wave mixing due to interaction-induced nonlinearities," *Phys. Rev. B*, vol. 54, pp. R14250, 1996.

[21] J. Erland, D. Birkedal, V. G. Lyssenko, and J. M. Hvam, "Spectral signatures of excitonic four-wave mixing signals in GaAs multiple quantum wells," *J. Opt. Soc. Am. B*, vol. 13, pp. 981, 1996.

[22] S. Adachi, "GaAs, AlAs, and Al/sub x/Ga/sub 1-x/As: material parameters for use in research and device applications," *J. Appl. Phys*, vol. 58, pp. R1, 1985.